Experimental determination of temperature threshold for melt surface deformation during laser interaction on iron at atmospheric pressure

Koji Hirano [1,2], Remy Fabbro [1], Maryse Muller [1]

[1] PIMM Laboratory (Arts et Métiers ParisTech-CNRS), 151 Boulevard de l'Hôpital 75013 Paris, France.

[2] Nippon Steel Corporation, Marunouchi Park Building, 2-6-1 Marunouchi, Chiyoda Ward, Tokyo 100-8071, Japan.

Email: hirano.koji@nsc.co.jp

Abstract. Recoil pressure is the principal driving force of molten metal in laser processing in the intensity range of 10^{-1} ~ 10^{2} MW/cm^2. It is thus essential to estimate the recoil pressure in order to describe physical processes or to carry out numerical simulations. However, there exists no quantitative estimation of the recoil pressure near the boiling temperature (T_v), which is particularly important in welding process. In this study we experimentally investigated the recoil pressure of pure iron around T_v. The main interest was to determine the threshold surface temperature to start deformation of melt surface. Using camera-based temperature measurement with accurate evaluation of emissivity from experiment, it was shown that the surface temperature has to reach T_v to initiate the melt surface deformation. This result provides the first experimental evidence for the frequently used assumption that a deep keyhole welding requires surface temperature over T_v. It is indicated also that, in normal gas-assisted laser cutting process, the recoil pressure hardly contributes to material ejection when the surface temperature is lower than T_v, as opposed to commonly believed presumption.

Keywords: Laser processing, Evaporation, Temperature measurement.

PACS: 42.62.-b, 81.20.-n, 47.80.Fg

1. Introduction

A number of laser metal processing such as welding, drilling, grooving utilise the intensity range of 10^{-1} ~ 10^{2} MW/cm^2, which are easily obtained by multi-kW class fibre, disk, Nd:YAG and CO_2 lasers. In this intensity range, materials are driven or removed in the form of liquid, while the fraction of vaporised material is limited. Understanding of hydrodynamics of molten material is thus essential to consider process efficiency or final quality achieved. Recoil pressure, which is sometimes called evaporation pressure or ablation pressure, is generated as a counter momentum to evaporation from the surface. It is widely accepted that the recoil pressure can be a dominant driving force of the molten material in various laser metal processing [1, 2], even though the evaporation itself contributes little to the mass removal.

It is well known that the recoil pressure exerted on the surface increases with the surface temperature T_s. One may then pose a question: what is the minimum surface temperature to

initiate the driving process of molten material? This question is very important, since this temperature determines limit of energy efficiency of various processes. Although there exist a few experimental measurements of the recoil pressure for several metal species [3-7], these are limited to the ablation regime with high laser intensity (typically > 1 MW/cm^2 for iron) well above the threshold of the ejection process. It should be noted also that in these studies, the recoil pressure was determined only as a function of laser intensity and it could not be related to the surface temperature. Consequently our understanding of the threshold temperature is not at all conclusive. Concerning a deep keyhole welding, for example, not a few studies have assumed that the keyhole surface temperature is equal to T_v [8-13], implying that this is the minimal temperature in order to carry out the keyhole welding process. In the well-known paper by Semak and Matsunawa [2], however, this assumption was denied. They claimed that the keyhole can be obtained at a temperature well below T_v. This kind of debates is caused by the lack of information on the temperature dependence of recoil pressure, especially in the region near T_v.

As for theoretical description of the recoil pressure, the expressions proposed by Anisimov [14] and Knight [15] have often been used for numerical studies of laser welding, drilling and cutting [2,16,17]. As explained in detail in the next section, an important assumption in their analyses is that the surrounding ambient gas does not touch the evaporating surface and thus does not contribute as a partial pressure to the total pressure at the evaporating surface. In this case, the total pressure is composed uniquely of the recoil pressure of metal evaporation. This assumption should be valid for the temperature range well above the boiling temperature T_v, where strong metal vapour jet emerging from the surface can completely expel the surrounding gas atoms. However, in the temperature range near T_v, where only weak evaporation takes place, the assumption is possibly not appropriate and the contribution of ambient gas may have to be considered to evaluate the total pressure exerted on the evaporating surface. But the problem is that, there exists no theoretical model that can take into account this contribution of the surrounding gas atoms to the total pressure at the surface in the case of laser processing under atmospheric ambient pressure. Experimental studies are thus required to clarify the temperature dependence of the total pressure at the surface.

Basu and DebRoy [18] and later He et al. [19] examined melt expulsion during laser spot welding of metals both experimentally and numerically. Their results indicated that ejection of spatters is initiated after melt surface temperature exceeds T_v. This hints that the total pressure at the surface becomes large enough to eject the melt layer only in the evaporation regime. The result, however, does not provide us precise information of the temperature dependence of the total pressure near T_v, because it is difficult to correlate the total pressure with the threshold of the spatter ejection. It should also be pointed out that the temperature distribution in their study was given by numerical simulations.

The present study investigates the total pressure exerted on the surface for the surface temperature range near T_v with experimental measurement of the temperature for the first time. Evolutions of surface shape and surface temperature are monitored with a high speed video camera during single impact irradiation on a pure iron sample. Special attention is paid to determination of the threshold temperature at which the surface starts to be deformed due to the pressure. This point should be contrasted with the above-mentioned works [18, 19], where the melt ejection, which occurs after the deformation, was analysed. Our focus on the small initial melt surface deformation allows us to evaluate the corresponding total pressure more precisely and to determine the threshold temperature for surface deformation in a more fundamental sense. Difficulty of the temperature measurement should be one of the factors that have prevented this kind of fundamental investigation on the pressure at the surface. In this work, thermal radiation

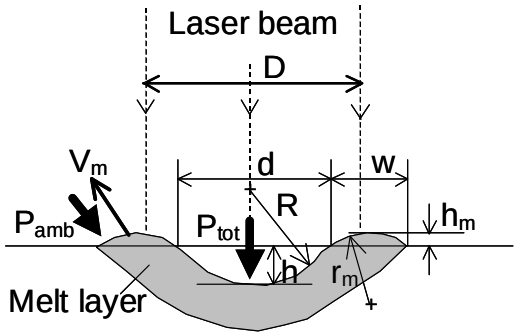

Figure 1 Pressure induced deformation of melt layer during irradiation of single laser pulse.

detected by the camera is processed using emissivity that is obtained experimentally, as reported in [20]. This accurate determination of emissivity enables us to reduce substantially error in the temperature measurement.

The outline of this paper is briefly summarised as follows. In the next section 2, theoretical aspects of the recoil pressure and the total pressure at the surface are described. The experimental methods of the surface shape and temperature measurements are explained in section 3, and the results are presented in section 4. In section 5 we discuss the consequences of the results on our understandings of physical processes during laser welding and cutting.

2. Theoretical background

It is schematically shown in figure 1 how the pressure applied on the surface deforms and ejects the molten material during a single laser pulse irradiation. We call the pressure measured at the laser beam centre the "total pressure" P_{tot} in this paper. It is called "total", because in general it is expressed as the sum of two partial pressures:

$$P_{tot} = p_r + p_g \quad (1)$$

where the first contribution p_r comes from the conventional recoil pressure as a counter force of metal evaporation from the surface and the latter p_g is the partial pressure of surrounding gas.

The value that is important to drive the melt is the pressure difference ΔP between P_{tot} at the centre and the pressure at the periphery of the melt layer. The latter can be given by the ambient pressure P_{amb}, because the periphery is normally out of the laser beam and so the evaporation does not occur. Thus

$$\Delta P = P_{tot} - P_{amb} \quad (2)$$

The ambient pressure P_{amb} can vary but is usually the atmospheric pressure (1.01×10^5 Pa).

Using (1) and (2), one obtains

$$\Delta P = p_r + p_g - P_{amb} \quad (3)$$

Please note that p_g is the partial pressure of surrounding gas measured locally at the target surface. Therefore, p_g can be different from P_{amb} and the two pressures do not generally cancel to each other.

The pressure difference ΔP is utilised to counteract the surface tension yielded from a deformation and to eject the material. Let us consider the case of figure 1, where the central part

is depressed due to ΔP and the melt in the centre is redistributed to the periphery as an extruded rim [21]. The curvatures of the melt deformation in the central and rim parts are expressed by R and r_m, respectively. As shown in figure 1, R and r_m are defined to be positive when the centres of the curvatures are situated above and below the melt surface, respectively. (In conditions of this study, both R and r_m become positive at any time.) When the melt is ejected from the rim with the velocity V_m, the pressure balance can be written using the Bernoulli equation.

$$\Delta P = \frac{2\sigma}{R} + \frac{\sigma}{r_m} + \frac{\rho_m V_m^2}{2} \tag{4}$$

Please note that the factor 2 in front of (σ/R) comes from the fact that the deformation at the centre consists of the two same curvatures along two orthogonal directions on the sample surface.

In the following, we will examine dependence of p_r and p_g in ΔP (eq.(3)) on the surface temperature T_s.

The recoil pressure p_r is a monotonously increasing function of the surface temperature T_s. Analytic expressions of p_r have been proposed by a number of authors. In a general form, the pressure can be approximated as [22]

$$p_r = \frac{1+\beta_R}{2} p_{sat}(T_s) \tag{5}$$

where p_{sat} is the saturated pressure at $T = T_s$. It can be obtained from the well-known Clausius-Clapeyron's relation:

$$p_{sat} = p_0 \exp\left(\frac{\Delta H_v}{k_B T_v}\left(1 - \frac{T_v}{T_s}\right)\right) \tag{6}$$

where T_v is the vaporisation temperature under the pressure p_0 and

$$\Delta H_v = mL_v \tag{7}$$

is the enthalpy of phase transition from liquid to vapour per atom (m: mass per atom, L_v: latent heat of vaporisation, $L_v = 6.1 \times 10^6$ J/kg for iron). The coefficient β_R represents the fraction of re-condensing particles to evaporating ones. By its definition, β_R is related to the mass flow balance. The total mass flux from melt layer to gas phase can be estimated from modified Langmuir expression [22, 23]:

$$\rho_m V_v = (1-\beta_R)\left(\frac{m}{2\pi k_B T_s}\right)^{1/2} p_{sat}(T_s) \tag{8}$$

Here k_B is the Boltzmann constant. β_R is influenced by gas flow of evaporating particles above the surface. It depends on T_s, P_{amb}, three-dimensional surface profile around the considered surface point, and so on. When $T_s \approx T_v$ it is expected that the evaporation is not so strong and $\beta_R \approx 1$ (so $p_r \approx p_{sat}$). With the increase of T_s, β_R decreases while the upward velocity of metal vapour flow increases until it reaches the sound velocity. In this limit, β_R becomes 0.18 [14,15,22]. According to eq.(5), $p_r = 0.6 p_{sat}$ in this regime. The equations (5) and (8) assume that atoms which recombine to the surface have the same temperature T_s as the evaporating ones. This assumption is valid only in weak evaporation regime where $\beta_R \approx 0$, but comparison with rigorous expressions in [15], which take into account temperature decrease of the recombining atoms, shows that the error of p_r caused by the approximate expression (5) is less than 10%.

Now let us consider p_g in eq.(3). It is considered that, when evaporation starts, p_g becomes smaller than P_{amb}, because evaporating metal particles reduces the number of surrounding gas atoms that impinge onto the surface. The only exception is processing under vacuum, where p_g

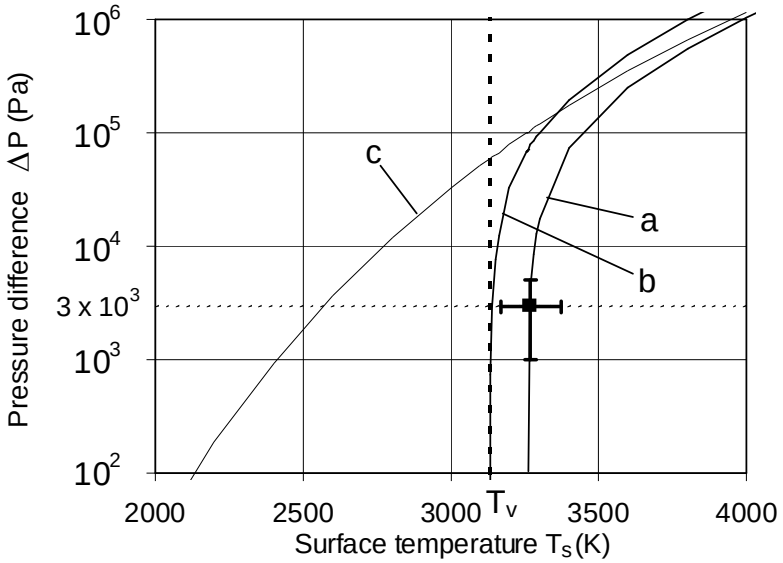

Figure 2 Pressure difference ΔP as function of the surface temperature T_s. The two curves a and b show theoretical equations in the case of processing of iron under $P_{amb} = 1.01 \times 10^5$ Pa (a: $\Delta P = 0.6p_{sat}(T_s) - P_{amb}$, b: $\Delta P = p_{sat}(T_s) - P_{amb}$). The curve a corresponds to the asymptotic curve in the limit of low β_R. The curve c shows the theoretical curve under vacuum conditions ($\Delta P = 0.6p_{sat}(T_s)$). The level of $\Delta P = 3 \times 10^3$ Pa corresponds to the minimal pressure difference needed to keep open a keyhole with the diameter of 1 mm. The rectangular dot (■) is the experimental point obtained in this work (see the sections 3-5 for details).

$= P_{amb} = 0$ at any T_s. In most cases, where a metal target is placed under atmospheric pressure of 1.01×10^5 Pa, the estimation of ΔP is rather complicated, due to the fact that p_g and P_{amb} do not cancel to each other. This point is important for the following discussions.

The characteristics of p_g and resulting ΔP can be estimated for the two extreme cases of low and high temperatures with respect to T_v. First let us consider the case where T_s is so small that $p_r \approx 0$ (see eqs.(5) and (6)). In this case, there are very few evaporating metal particles. It can thus be assumed that $p_g = P_{amb} = 1.01 \times 10^5$ Pa. From eq.(3) one obtains $\Delta P = p_r \approx 0$, which means that there is no driving force of molten material. On the other hand, if T_s reaches the strong evaporation limit of $\beta_R = 0.18$, the intense metal vapour flow prevents the surrounding gas atoms from reaching the surface. Thus $p_g \approx 0$ and consequently $\Delta P \approx p_r - P_{amb} = 0.6p_{sat} - P_{amb}$. In figure 2, ΔP in this limit is shown with the curve a for the case of iron. The problem is that we do not have enough information on ΔP in the intermediate temperature range near T_v, where with the increase of T_s, p_g decreases from P_{amb} to zero and p_r gains from zero depending on the magnitude of the unknown parameter β_R.

There exists no theoretical model that can predict this variation of ΔP around T_v in the case of processing under ambient pressure. The first analytical model by Anisimov [14] was limited to the case of vaporisation into vacuum. Knight proposed another model [15], which can take into account the existence of ambient gas. It was assumed, however, that ambient gas is completely screened out from the evaporating surface by metal vapour that covers totally the surface, which corresponds to the case of $p_g = 0$. As mentioned above, this assumption should be valid in strong evaporation regime, but its validity is not conclusive for weak evaporation in the vicinity of T_v.

The consideration of mixing of the ambient gas and the metal vapour is still a challenging problem even with modern numerical techniques and there are very few works. Bellot and co-workers [23] numerically solved the Boltzmann equation to study the influence of surrounding gas pressure and geometrical scale factor for the evaporation problem of Cr from iron liquid. Unfortunately, the partial pressure of the surrounding gas they used, was limited approximately under 100 Pa. Due to the lack of theoretical model, experiments are indispensable to estimate the pressure ΔP in the temperature region near T_v.

It should be pointed out that little attention has been paid to the contribution of ambient gas on ΔP, which has been proposed as in eq.(3). In a number of papers dealing with recoil pressure during laser material processing, the following type of expressions has been used.

$$\Delta P = p_r \tag{9}$$

This should be a good approximation, when T_s is so high that $p_g = 0$ and $p_r >> P_{amb}$. However, in order to describe lower temperature regime, such as the regime of a deep penetration keyhole welding, the validity of eq.(9) must be questioned, since it implicitly assumes that $p_g = P_{amb}$. As already mentioned, in the case of processing under atmospheric pressure, p_g must decrease from P_{amb}, when evaporation starts.

3. Methods of experiments

Schematic of the experimental setup is shown in figure 3. We investigated evolutions of surface shape and temperature during a single impact irradiation. The position of the laser beam was fixed during each irradiation. A disk laser (Trumpf, TruDisk10002) was utilised as the laser beam source. A non-polarised laser beam with the wavelength λ_L of 1030 nm, which was transmitted through an optical fibre with the core diameter of 600 μm, was imaged on a workpiece with a combination of a collimator lens (f = 200 mm) and a focusing lens (f = 560 mm). The obtained focus diameter was 1.6 mm and the focus position was always set at the sample surface. The beam profile at the focus position was analysed with a commercial CMOS camera and the top-hat distribution of the intensity was confirmed. The samples were pure iron (Goodfellow FE000480; purity 99.95%). Their surfaces were polished with sand papers (# 2400) and cleaned with ethanol before the laser irradiation. Argon gas was provided as shielding gas to avoid undesirable oxidation. Different configurations were used to observe the evolutions

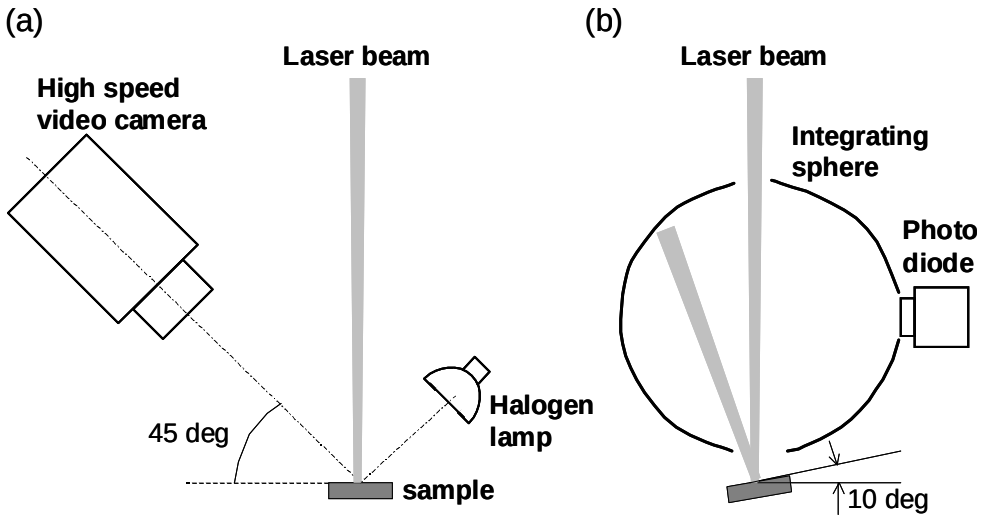

Figure 3 Schematics of the experimental setups for the observation of melt surface deformation or the measurement of NIR radiation from the surface (a), and for the absorptivity measurement (b).

of surface shape and surface temperature, with the above-mentioned processing conditions fixed.

As for the observation of the surface shape, we illuminated the surface with a halogen lamp and observed a reflected image with a high speed video camera (Photron, FASTCAM/APX-RS). As shown in figure 3(a), the angles of the illumination and the observation are set at 45 degrees. The spatial resolution per pixel was 6.0 μm x 8.5 μm. We placed a standard glass filter of the type KG3 in front of the camera lens to block the laser beam reflected from the irradiation spot. Therefore the whole visible spectrum region was utilised. The acquisition rate was set at 20 kHz and the shutter speed was 2 μs.

Two-dimensional distribution of surface temperature was monitored using a camera-based technique, which was reported for example in [20]. Thermal radiation from the surface was detected by a high speed video camera. Based on the Planck's law, the surface temperature was calculated from the measured radiation level and the emissivity that was obtained experimentally.

Thermal radiation level was measured with a CMOS sensor of the above-mentioned high speed video camera. We used the same optical system, observation angle (45 degrees) and acquisition rate as the observation of the surface shape, which allowed us the high spatial resolution (6.0 μm x 8.5 μm) and sampling rate (20 kHz). The differences from the surface shape observation were: we did not use the lamp for illumination; we selected a near infrared (NIR) spectrum band as specified below; and we used an adapted shutter speed (50 μs).

According to the Planck's radiation theory, the grey scale level G measured at a pixel of the CMOS sensor is generally expressed as

$$G = K\varepsilon(\lambda_0, T)B(T) \tag{10}$$

K is a constant, which depends on characteristics of the observation system, for example, numerical aperture of the lens system, transmittance of the thermal radiation from the laser spot to the sensor surface, shutter speed and the sensibility spectrum of the sensor. $\varepsilon(\lambda_0, T)$ is the emissivity of the surface at the central wavelength λ_0 of the spectrum band selected. B(T) represents the temperature dependence of the black body radiation

$$B(T) = \int_{\lambda_0 - \Delta\lambda/2}^{\lambda_0 + \Delta\lambda/2} d\lambda \frac{2hc^2}{\lambda^5} \frac{1}{\exp\left(\frac{hc}{\lambda k_B T}\right) - 1} \tag{11}$$

where $\Delta\lambda$ is the width (FWHM) of the selected band, and h and c are the Planck constant and the speed of light, respectively. B(T) can easily be calculated from eq.(11), so that once the constant K and ε are obtained, the surface temperature T can be determined from the grey scale level G.

The emissivity ε is a function of wavelength and of temperature, which is then a function of time. Based on the Kirchhoff's law, the temporal evolution of ε was estimated from that of the absorptivity A, which was evaluated for the process laser wavelength λ_L (1030 nm), assuming that

$$\varepsilon(\lambda_0, T(t)) \approx A(\lambda_L, T(t)) \tag{12}$$

It can be mentioned here that this correspondence of ε and A has been recently utilised for monitoring of keyhole front profile during laser welding [24]. Considering that ε in (12) depends on the wavelength, it is better to use λ_0 near λ_L and small $\Delta\lambda$ for the NIR radiation

observation by the video camera. We selected a spectrum band of $\lambda_0 = 0.9$ μm and $\Delta\lambda = 0.07$ μm using a band pass filter.

The setup for the measurement of A is shown in figure 3(b). The sample was placed just under an integrating sphere for the measurement. More details of the absorptivity A variation with operating parameters will be discussed in a future publication. For the present study, the evolution of A was measured using exactly the same laser power and duration as those of the NIR radiation observation. The incidence angle was set at 10 degrees in order to capture the first reflection from the sample within the sphere. The angle was different from that of the NIR observation (45 degrees), but the influence is negligibly small. According to the theoretical Fresnel formula and the complex refraction index of iron, the difference of ε (or A) between 10 degrees and 45 degrees is very small for a non-polarised beam; less than 1% [25].

The constant K of this observation system was calibrated at the melting points of Ta (3290 K) and Nb (2750 K) through the same scheme of the evaluations of G and A as the measurement for pure iron. As is deduced from eq.(10), systematic error in a measured temperature can come from errors in K and ε. The error in the determination of K in the calibration processes with Ta and Nb was about +/-7 % (= $\Delta K/K$). This leads to the error of +/-50 K in T_s if it is evaluated at $T_s \sim T_v$. The experimental measurement of A allowed us to minimise the error of ε within +/-3 %, which corresponds to the error of +/-50 K in T_s. By adding the two contributions, the total error in T_s is estimated to be +/-100 K.

The present method of temperature measurement applies only to the case where the deformation is so small that one observes only a component of NIR light that is emitted from the surface and directly transferred to the video camera. When the deformation becomes large, for example, as in the case of a keyhole, reflected component, which is emitted from another point, can be overlapped to the observed light in addition to the direct emission. The method in this study is based on a presumption that there is no such contribution from these reflections. In order to measure temperature also for the case where single or multiple reflections occur, it would be necessary to make the observation of the NIR image with the same angle as the incidence angle of the absorptivity measurement, for example, by installing the camera coaxially to the laser beam axis.

While a laser pulse is irradiated on the sample surface the surface temperature T_s is continuously elevated or stagnated. The surface shape strongly depends on ΔP (= P_{tot} - P_{amb}), which is a function of T_s as explained above. Although the evolution of T_s is a dynamic phenomenon, it is considered that P_{tot} is dependent only on the instantaneous value of T_s, independent from any dynamical factor. This assumption is justified because the time needed for equilibrating P_{tot} for each instance is estimated to be as small as the order of 20 μs, if one estimates from (L/v_s) [26], where L is the characteristic relaxation length of the uprising vapour ($\lesssim$ 10 mm) and v_s is the sound velocity ($\approx$ 500 m/s). As shown later, the characteristic time of the evolution of T_s is much longer in our experimental conditions.

Apart from the observations of deformation and temperature, in order to estimate the recombination rate β_R in the eqs.(5) and (8), mass loss by evaporation was evaluated by measuring weight of samples before and after irradiation using a commercial balance (METTLER TOLEDO AT261). The precision of each weight measurement was +/-0.02 mg. Using the high speed video camera we confirmed that there was no droplet detached from the surfaces during the laser beam irradiation, which would have caused overestimation of the evaporation rate.

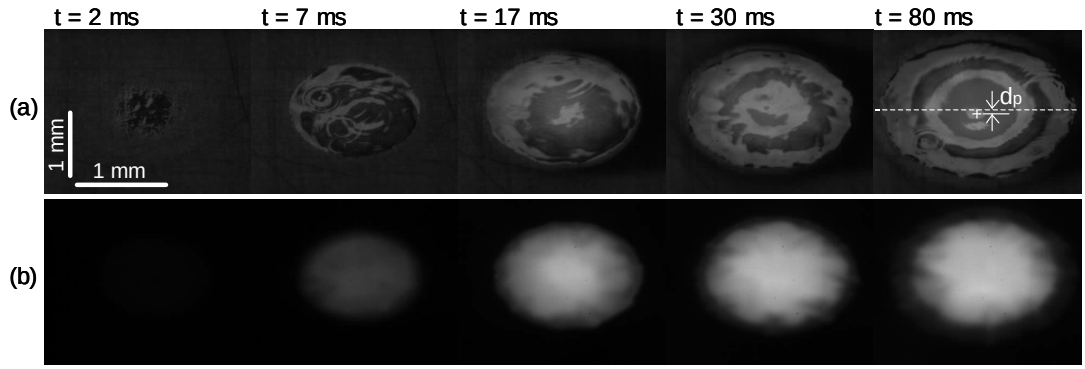

Figure 4 Temporal evolutions of surface shape (a) and NIR emission (b) observed with the high speed video camera in the case of P = 2 kW and Δt = 80ms. In the image at t = 80 ms of (a), it is observed that the centre of the circular deformed region (cross mark) is displaced by d_p from the initial level of the central line on the surface (dotted line). This value was used to estimate the depression depth h at the centre ($h \approx d_p$).

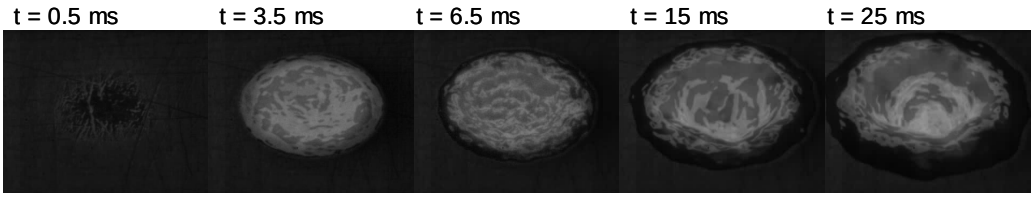

Figure 5 Temporal evolution of surface shape for P = 4 kW and Δt = 25 ms. The scale of the images is the same as figure 4.

4. Results

4.1 Evolution of melt surface shape

Depending on the level of T_s, and thus on the level of P_{tot}, we can observe the melt pool evolution during the pulse irradiation in three stages: (i) flat, (ii) deformation, and (iii) key-hole. In the following, two typical conditions are shown. One is P = 2 kW, Δt = 80 ms, for which the system stagnates in the stage (ii). In the other condition of P = 4 kW, Δt = 25 ms, the system gets into the final keyhole stage (iii).

The evolution of surface shape observed for P = 2 kW and Δt = 80 ms is shown in figure 4(a). Please note that information on surface profile tends to be amplified with the illumination by the halogen lamp. From the observed video images, it was confirmed that melting starts at time t = 1.7 ms from the centre of the laser beam spot. The melted region spread with the elapse of time after that. In this first stage the liquid surface stays almost flat but is never stationary. As shown in the image of t = 7 ms, ring patterns, such that we observe when a raindrop plunges into water surface, were frequently observed. The detection of this phenomenon was made possible owing to the fast shutter speed of the camera (2 μs).

The second regime sets in at t = 17 ms, when one can confirm the initiation of concave deformation in the centre. The diameter d and the depth h of the deformation area gradually increase with time until the end of the pulse. The depth h was estimated from small displacement of the centre of the circular deformed region that can be observed due to the

inclined angle of visualisation of the high speed video camera (Figure 3(a)). Due to the inclination angle of 45°, h can be estimated by the displacement distance d_p of the centre measured in the plane of the sample surface (refer to an example at t = 80 ms in figure 4(a)). At t = 60 ms, the diameter d of the deformed region was 1.1 mm +/- 0.2 mm and the depth h was 80 μm +/- 20 μm.

Let us estimate the pressure difference ΔP from the values d and h measured at t = 60 ms. Using eq.(4) with the ejection velocity $V_m = 0$, the pressure difference ΔP is estimated from the following equation

$$\Delta P \approx \frac{2\sigma}{R} + \frac{\sigma}{r_m} \tag{13}$$

The curvature R of the liquid surface at the bottom can be estimated from the geometrical formula $R = ((d/2)^2 + h^2)/2h$, which gives R = 2 +/- 1 mm. In order to estimate the curvature r_m of the rim, we assume that the rim extruded above the sample surface is represented by a part of a torus which is cut at the sample surface, as in ref. [21]. This extruded volume should be provided from the depressed volume in the central part. This volume balance can be approximated as

$$\frac{1}{3}\pi\left(\frac{d}{2}\right)^2 h \approx \left(\frac{1}{2}wh_m\right) \times 2\pi\left(\frac{d}{2} + \frac{w}{2}\right) \tag{14}$$

The width w is measured to be 0.5 +/- 0.1 mm from the image at t = 60 ms. Substituting this value to eq.(14), one obtains $h_m \approx 0.02$ +/- 0.01 mm. Then r_m is estimated to be 1.5 +/- 1 mm from the geometrical formula $r_m = ((w/2)^2 + h_m^2)/2h_m$. Using $\sigma \approx 1.5$ Pa m, we finally obtain $\Delta P \approx 3$ +/- 2 x 10^3 Pa. (We neglect temperature dependence of σ.)

Images observed with P = 4 kW and Δt = 25 ms are shown in figure 5. Melting starts at t = 0.4 ms, and the second deformation stage begins at t ≈ 4 ms. The concaved surface is modulated with small wavy structure as one can confirm in the image of t = 6.5 ms. Unlike the case of P = 2 kW, the evolution of the surface profile is not stationary, and finally at t ≈ 15 ms, a keyhole is produced.

4.2 Evolution of melt surface temperature

Because the method of temperature measurement cannot be applied to the case of strong deformation, we present only the result for the condition of P = 2 kW and Δt = 80 ms. Observed NIR images are shown in figure 4(b). Results of the absorption measurement and the calculated surface temperature T_s are plotted in figure 6 as a function of time. The grey scale level G was evaluated as an average in a small circle at the beam centre with the diameter of 0.2 mm. Variation of the temperature within the circle was typically +/- 10 K. Considering that this variation can generally be caused by real temperature variation and/or noise of each pixel, it can be said that the value (+/- 10 K) defines the maximal value of the temperature variation.

As shown in figure 6, the temperature T_s in the central region increases and reaches T_s = 3250 K at t = 17 ms and stagnates after that at about T_s = 3270 K. This characteristic rising time of T_s can be explained by the following 1D analytical solution of heat conduction problem for surface heating of a semi-infinite body with constant intensity [27]. The temperature increase at the centre on the surface is given by

$$T_s - T_a = \frac{2AI_L}{K}\sqrt{\frac{\kappa t}{\pi}} \tag{15}$$

where I_L is the incident laser intensity (0.1 MW/cm^2), K is the heat conductivity (80 W/m K), κ

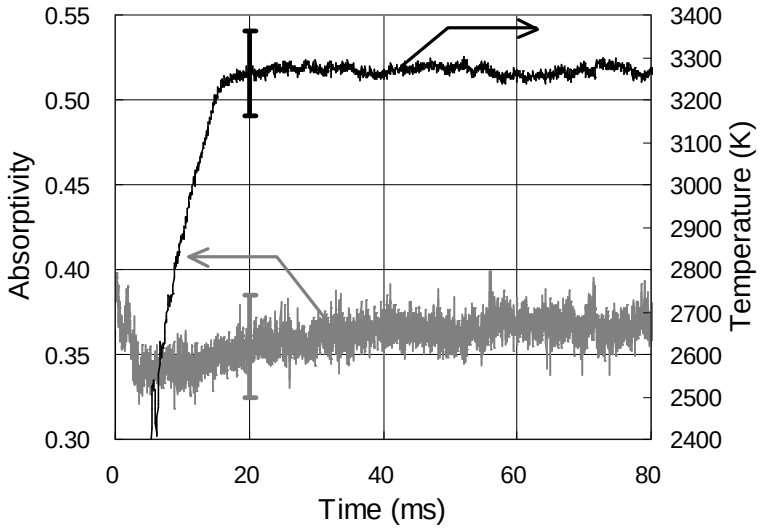

Figure 6 Results of measurements of absorptivity and surface temperature in the case of P = 2 kW and Δt = 80ms.

is the thermal diffusivity (2 x 10^{-5} m^2/s), and T_a is the ambient temperature (300 K). This 1D equation neglects three-dimensional thermal diffusion, which is estimated to start at $\tau \sim 10$ ms based on the relation $2(\kappa\tau)^{1/2} \approx (D/2)$. We neglect the latent heats of melting and evaporation in this discussion. The assumption of no evaporation is justified, since it was experimentally confirmed that evaporated mass is negligibly small until t = 17 ms, as is shown later. Using the experimentally obtained absorptivity ($A \approx 0.35$), the rising time to T_s = 3250 K is estimated to be 17 ms, which shows a good agreement with the experiment in spite of the approximations.

The observation of surface shape showed that the surface deformation starts at t = 17 ms. Thus the threshold surface temperature for the melt surface deformation is determined to be 3250 K +/- 100 K. It can be concluded that the surface deformation starts just above T_v (3134 K).

Whereas T_s at the centre stagnates, the 2D temperature field continues to evolve even after t = 17 ms. Further analysis showed that the region with the maximum temperature (= 3270 K) slightly spreads with time until $t \approx 60$ ms. The diameter of this region stays constant at about 0.5 mm for t = 60 ~ 80 ms. The temperature distribution was quasi-stationary during this period.

4.3 Evaporation rate

Mass loss by evaporation measured for the case of P = 2 kW and Δt = 80 ms is shown in figure 7. Comparison with the evolution of T_s suggests that the mass loss by the evaporation only starts after T_s surpasses T_v. The mass loss rises roughly proportionally to the pulse duration after this moment. The mass evaporation rate in the quasi-stationary regime (t = 60 ~ 80 ms) can be determined as $\dot{m}$ = 1.4 x 10^{-5} kg/s from the gradient of the plots. Based on the modified Langmuir eq.(8), the recombination rate β_R was calculated from the following relation

$$\beta_R = 1 - \frac{\dot{m}}{\int \left(\frac{m}{2\pi k_B T_s} \right)^{1/2} p_{sat}(T_s) dS} \qquad (16)$$

with the expression of p_{sat} taken from eq.(6) and the integrated area defined by the beam diameter. For T_s, the temperature distribution at t = 60 ms was used. The obtained

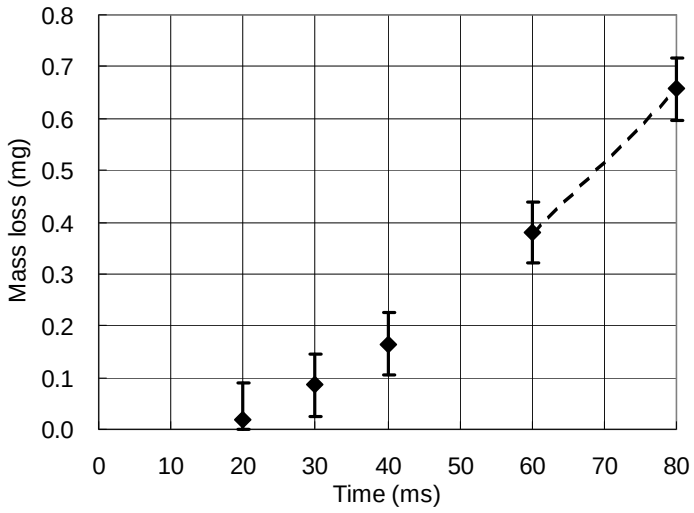

Figure 7 Results of measurement of evaporated mass in the case of P = 2 kW and Δt = 80ms.

recombination rate β_R was 0.9.

Now let us discuss about the stagnation of T_s at the centre observed after t = 17 ms. It is considered that the stagnation of T_s at the centre is caused by increase of three-dimensional thermal diffusion and reduction of heat flux into the sample due to evaporation heat loss. If we consider surface heating of a semi-infinite body with a circular beam that has the intensity I_{abs} and the diameter D, the analytical solution predicts that the temperature increase at the centre stagnates at (I_{abs}D/2K) because of the heat conduction. Taking also into account the reduction of the incoming energy flux due to evaporation loss, the temperature increase in the stationary regime is estimated from

$$T_s - T_a = \frac{2\left(AP_L - \dot{m}L_v\right)}{\pi DK} \qquad (17)$$

This equation gives T_s = 3.5 x 10^3 K, which is close to the stagnation level observed experimentally.

5. Discussion

5.1 Temperature dependence of ΔP

As explained above, the pressure difference ΔP at t = 60 ms is estimated to be ΔP ≈ 3 +/- 2 x 10^3 Pa, from the result of the surface shape observation. The measurement of surface temperature shows that T_s is quasi stationary at 3270 K around t = 60 ms. These results add an experimental point in figure 2, which shows the dependence of ΔP on T_s for the case of processing under P_{amb} = 1.01 x 10^5 Pa. The important conclusion is that the melt surface deformation or the melt ejection due to the recoil pressure is obtained only above T_v, where ΔP becomes large enough. This finding allows us to understand better physical processes during laser welding and cutting, as discussed below in the sections 5.2 and 5.3.

The recombination rate determined from the mass loss measurement (β_R = 0.9) may seem to be high, but similar results can be found in the past works. Mundra and DebRoy [28] measured mass evaporation rate during conduction mode laser welding of stainless steel. It was reported

that the evaporation rate of iron was only 15% of the value predicted from the Langmuir equation at $T_s \approx 3200$ K, which is about the same as the temperature in our case (3270 K), although their temperature was not measured experimentally but estimated from a numerical simulation. The rate β_R in their work was 0.85, which is very close to our result. As for numerical investigations of β_R, Bellot et al. [23] studied the dependence of β_R on ambient Ar pressure for evaporation of Cr from liquid iron surface in near vacuum condition. It was shown that, when the Ar pressure becomes comparable to the saturated pressure of Cr, β_R for Cr evaporation rises up and approaches 1. These previous results support the rather high value of β_R obtained in this study.

It must be mentioned, however, that the experimentally obtained ΔP and β_R at $T_s = 3270$ K are not completely consistent with the theoretical prediction. Indeed, using $\beta_R = 0.9$ obtained at $T_s = 3270$ K, p_r is calculated to be 1.6×10^5 Pa from eq.(5). Considering that $P_{amb} = 1.0 \times 10^5$ Pa and $p_g \geq 0$, the right hand side of eq.(3) is equal to or larger than 6×10^4 Pa, which is larger than ΔP ($= 3 \times 10^3$ Pa). The errors in the experimental measurements of T_s and $\dot{m}$ might have caused this inconsistency. Nevertheless, the fact that the term $(p_r - P_{amb})$ in the right hand side of the eq.(3) is already larger than ΔP suggests that $p_g \approx 0$. This means that the shielding Ar atoms are expelled from the surface of the beam spot already at $T_s = 3270$ K. This indicates that the effect of the ambient atmospheric pressure at $T_s \sim T_v$ is not the direct contribution as the partial pressure to the total pressure at the surface, but the confinement of metal vapours, which results in the high value of β_R (= 0.9) compared with the vacuum case ($\beta_R = 0.18$).

Now let us discuss about the expression of ΔP as a function of T_s. Assuming that $\beta_R = 0.9$ and $p_g = 0$, the pressure difference ΔP in the range of $T_s \sim T_v$ may be expressed as $(0.95 p_{sat}(T_s) - P_{amb})$, which is very close to the curve b $(p_{sat}(T_s) - P_{amb})$ in figure 2. As already mentioned in section 2, when T_s increases from T_v, it is predicted that β_R decreases down to 0.18 and correspondingly ΔP approaches $(0.6 p_{sat}(T_s) - P_{amb})$, which is shown with the curve a in figure 2. Further investigation on the dependence of β_R on T_s is out of the scope of this work, it may be worthwhile to mention that the asymptotic convergence at high temperature depends more or less on geometry around the considered surface point. Aden et al. [29, 30] theoretically analysed metal vapour expansion dynamics in 3D geometry. It was shown that with the increase of the laser intensity and that of T_s, β_R approaches ~ 0.2. It was also revealed that, when the beam diameter becomes larger, β_R reaches this limit at higher laser intensity and that this delay is most pronounced at the extreme of 1D case. Similar effect of evaporating surface size on the magnitude of β_R was also reported in [23]. It was shown that, when the area of the evaporating surface becomes small, one needs higher ambient pressure of Ar to restrict the evaporating mass of Cr, that is, to keep β_R at a high level. Apart from this surface size effect, we point out that the global geometry can also influence β_R. For example, in the case of a deep keyhole welding, it is considered that β_R effectively increases, since metal atoms vaporised from a keyhole wall can be absorbed again to the other side of the wall surface. As a result, ΔP will reach the strong evaporation limit of $(0.6 p_{sat}(T_s) - P_{amb})$ at higher T_s compared with an open geometry.

As for practical interests such as boundary conditions of pressure for numerical simulations of melt pool dynamics driven by the recoil pressure, the variation of β_R from 1 to 0.18 with increase of T_s is possibly not so important, because the temperature difference between the curves a and b for a certain ΔP level is only ~ 100 K, as shown in figure 2. Therefore, it can be sufficient to use the curve a $(0.6 p_{sat}(T_s) - P_{amb})$ with extrapolation down to $T_s \sim T_v$, if one accepts the corresponding error. The measured point ($\Delta P = 3 \times 10^3$ Pa at $T_s = 3270$ K), which lies near the curve a, supports the validity of this approximation. It should be emphasised that, in order to conduct accurate simulations, what is much more important than the variation of β_R is to really

take into account the ambient atmospheric pressure P_{amb}, as discussed below.

5.2 Welding

The present result allows us to correct our common understandings on some processes in which T_s becomes comparable to T_v. First let us discuss consequence on a deep penetration keyhole welding. The minimum pressure difference ΔP to carry out a keyhole welding can be estimated from the following relation.

$$\Delta P \approx \frac{2\sigma}{d_k} + \frac{\rho_m V_m^2}{2} \tag{18}$$

where d_k is the diameter of the keyhole. For example, if we take d_k = 1 mm and consider the limit of low velocity ($V_m \approx 0$), $\Delta P = 3 \times 10^3$ Pa. According to figure 2, it is predicted that T_s must be at least in the order of T_v to keep the keyhole open. In theoretical analyses of a deep penetration keyhole welding, it has often been assumed that the temperature T_s of the keyhole surface is equal to T_v. The present result provides the first experimental support to this assumption.

We have to point out, however, that this assumption has been sometimes doubted in the past. For example, Semak and Matsunawa [2] denied this assumption and claimed that the recoil pressure can trigger lateral ejection at a lower temperature even near the melting temperature. Using the Bernoulli type equation (the equation number (10) in [2])

$$p_r = \frac{\rho_m V_m^2}{2} \tag{19}$$

they claimed that a meaningful ejection velocity can be obtained even for $T_s < T_v$. As already discussed in section 2, the equation (19) is based on the implicit assumption that $p_g = P_{amb}$. This assumption is not correct according to the present result which suggests that $p_g \approx 0$ at the threshold temperature for melt surface deformation.

It is predicted that the threshold temperature for keyhole welding strongly depends on the ambient pressure. In figure 2, we plot $\Delta P = p_r$ for the extreme case of processing under vacuum, assuming that $\beta_R = 0.18$ (the curve c in figure 2). ΔP can take non-zero value even when $T_s < T_v$. For example, the above-discussed deep keyhole welding with the diameter of 1 mm, which requires $\Delta P = 3 \times 10^3$ Pa, will be realised at $T_s \approx 2600$ K. This decrease of the process temperature must be one of the reasons why the penetration depth achieved in a deep penetration welding under vacuum is larger than the case under the atmospheric pressure for the same laser condition [31, 32].

The same discussion applies also to boundary condition of pressure in numerical simulations of a keyhole welding process, which have already been reported by several groups [16,17,33]. The result of our study highlights the importance of imposing the ambient atmospheric pressure P_{amb} to non-evaporating surfaces, although this boundary condition was not clearly described in these papers. If one omits P_{amb} for the non-evaporating surfaces, the calculation will represent the case of welding under vacuum, and it will predict that surface temperature threshold for keyhole regime can be lower than T_v.

5.3 Cutting

We have to correct our understanding also for laser cutting process. In some of the analytical models for laser cutting, the recoil pressure P_{recoil} have been taken into account as an important mechanism of melt ejection in lateral direction from the kerf front to the side region [34-36]. It has been shown that the fraction of the lateral ejection can be the same order as that of the longitudinal ejection by downward assist-gas force, even when the surface temperature T_s is

well below T_v [34, 37]. Our present result shows, however, that the lateral ejection by the recoil pressure cannot occur when $T_s < T_v$. A recent experimental investigation of temperature distribution on the kerf front [38] indicates that T_s reaches T_v only for relatively high cutting speed near the process limit and this is restricted in a bottom part of the kerf. The absence of lateral ejection suggests that the downward melt flow by assist gas should be the only principal mechanism of melt ejection from the kerf. This was supported by our recent observation [39] that the melt flows downwards with little lateral velocity component except for a high velocity range where T_s is possibly comparable to T_v. In the lowest velocity range, we observed interaction between melt accumulations in the central and side parts of the kerf front [39]. It should be noted, however, that this interaction does not originate from the recoil pressure but from surface tension. Of course, the lateral ejection induced by the recoil pressure can be important when the surface temperature T_s becomes higher than T_v. For instance, in remote laser cutting of steel, where assist-gas is not utilised, the ejection by the recoil pressure should be the principal mechanism of melt removal from kerfs. Also in the case of normal gas assisted cutting, it is reported that the lateral ejection occurs depending on the surface temperature in pulsed laser cutting of ceramics [36].

5.4 Future prospects

Whereas only pure iron samples were utilised in this study, it will be interesting to investigate the recoil pressure using practical materials with impurity elements. It is well acknowledged that volatile elements, which have lower boiling temperature than matrices, can cause process instabilities and defects. Fundamental investigations of the effect of additional elements on the characteristics of the recoil pressure will serve to understand the mechanisms of these problems.

We demonstrated a fast 2D measurement of melt surface temperature up to the range near T_v. This technique can also be applied to real time process monitoring or to development of numerical models, although at the present stage the technique is restricted to relatively flat surface, for example, melt surface around a keyhole. An important finding in this study is that the emissivity is almost independent of T_s up to ~ T_v. Consequently, even without measurement of the emissivity, one can estimate T_s with reasonable accuracy from thermal radiation intensity detected by a 2D sensor.

6. Conclusion

In this work we studied recoil pressure of iron around its boiling temperature T_v during laser processing under atmospheric pressure. Single laser pulse irradiation on iron was experimentally investigated with a specific aim to determine the threshold temperature of the melt surface deformation. The camera-based 2D temperature measurement technique, where thermal radiation intensity was processed by emissitivity obtained from experiments, was applied for the first time to investigate the fast evolution of melt surface temperature T_s up to the evaporation regime. It was revealed that the deformation starts at T_s = 3250 K +/- 100 K, which is just above T_v. Furthermore, the experimental determination of the recombination rate β_R in the evaporation process clarified the role of ambient atmospheric pressure on the total pressure exerted on the surface. That is, at T_s ~ T_v, ambient gas atoms do not contribute to the total pressure at the surface by direct impingement, but they confine metal vapours, which results in the increase of the recombination rate β_R. The determination of the threshold temperature for melt surface deformation leads to some important conclusions for physical mechanisms in practical laser processing. It provides the first experimental support for the assumption that the temperature on the keyhole surface during deep penetration laser welding must be at least T_v. As for laser cutting, it is suggested that lateral melt ejection process should be negligible as far as T_s does not reach T_v.

Acknowledgements
The authors would like to thank S. Kojima (PHOTRON LIMITED) and M. Sugiura (Nippon Steel Corporation) for useful advice about the temperature measurement.

References:

[1] M. Von Allmen 1987 *Laser-Beam Interactions with Materials* (Berlin, Springer)
[2] Semak V and Matsunawa A 1997 The role of recoil pressure in energy balance during laser materials processing *J. Phys. D:Appl. Phys.* **30** 2541-2552
[3] Kuznetsov L I 1994 Recoil momentum at a solid surface during developed laser ablation *Quantum Electron* **23** 1035-1038
[4] Batanov V A, Bunkin F V, Prokhorov A M and Fedorov V B 1973 Evaporation of metallic targets caused by intense optical radiation. *Sov. Phys. JETP* **36** 311-322
[5] Apostol I, Vatanov V A, Mikheilesku I N, Morzhan I, Prokhorov A M and Fedorov V B 1976 Recoil impulse received by metal targets as a result of interaction with microsecond CO_2 laser radiation *Sov. J. Quantum Electronics* **6** 1119-1120
[6] Golovin A F and Petrukhin A I 1985 Some features of the evaporation of magnesium and lead by quasi-cw laser radiation. *Sov. J. Quantum Electron.* **15** 846-848
[7] Lee D J and Jeong S H 2004 Analysis of recoil force during Nd:YAG laser ablation of silicon *Appl. Phys. A* **79** 1341-1344
[8] Dowden J, Davis M and Kapadia P 1985 The flow of heat and the motion of the weld pool in penetration welding with a laser *J. Appl. Phys.* **57** 4474-4479
[9] Kaplan A 1994 A model of deep penetration laser welding based on calculation of the keyhole profile *J. Phys. D: Appl. Phys.* **27** 1805-1814
[10] T J Colla, M Vicanek and G Simon 1994 Heat transport in melt flowing past the keyhole in deep penetration welding *J. Phys. D: Appl. Phys.* **27** 2035
[11] Solana P and Ocana J L 1997 A mathematical model for penetration laser welding as a free-boundary problem J. Phys. D: Appl. Phys. **30** 1300-1313
[12] Zhao H and DebRoy T 2003 Macroporosity free aluminum alloy weldments through numerical simulation of keyhole mode laser welding *J. Appl. Phys.* **93** 10089
[13] Le Guen E, Carin M, Fabbro R, Coste F and Le Masson P 2011 3D heat transfer model of hybrid laser Nd:Yag-MAG welding of S355 steel and experimental validation *Int. J Heat Mass Transfer* **54** 1313-1322
[14] Anisimov S I 1968 Vaporization of Metal Absorbing Laser Radiation *Sov. Phys. JETP* **27** 182-183
[15] Knight C J 1979 Theoretical Modeling of Rapid Surface Vaporization with Back Pressure *AIAA J* **17** 519-523
[16] Ki H, Mohanty P S and Mazumder 2002 J Modeling of Laser Keyhole Welding: Part I. Mathematical Modeling, Numerical Methodology, Role of Recoil Pressure, Multiple Reflections, and Free Surface Evolution. *Metall. Mat. Trans. A* **33A** 1817-1830
[17] Pang S, Chen L, Zhou J, Yin, Y and Chen T 2011 A three-dimensional sharp interface model for self-consistent keyhole and weld pool dynamics in deep penetration laser welding. *J. Phys. D: Appl. Phys.* **44** 025301
[18] Basu S and DebRoy T 1992 Liquid metal expulsion during laser irradiation *J. Appl. Phys.* **72** 3317-3322
[19] He X, Norris J T Fuerschbach P W and DebRoy T 2006 Liquid metal expulsion during laser spot welding of 304 stainless steel *J. Phys. D: Appl. Phys.* **39** 525-534
[20] Kraus H G 1986 Optical spectral radiometric method for measurement of weld-pool surface temperatures *Optics Letters* **11** 773-775
[21] Semak V V, Knorovsky G A, MacCallum D O and Allen Roach R 2006 Effect of surface tension on melt pool dynamics during laser pulse interaction *J. Phys. D: Appl. Phys.* **39** 590-595
[22] Samokhin A A 1990 First-order phase transitions induced by laser radiation in absorbing

condensed matter. In Proceedings of the Institute of General Physics (Ed. by Prokhorov A M), Vol. 13: Effect of laser radiation on absorbing condensed matter (Commack, Nova Science Publishers) pp.1-161
[23] Bellot J P, Duval H, Ritchie M, Mitchell A and Ablitzer D 2001 Evaporation of Fe and Cr from Induction-stirred Austenitic Stainless Steel. Influence of the Inert Gas Pressure *ISIJ International* **41** 696–705
[24] Weberpals J, Schuster R, Berger P, Graf T 2010 Utilization of Quantitative Measurement Categories for Process Monitoring *Proc ICALEO* (Anaheim, CA) 44-52
[25] Dausinger F and Shen J 1993 Energy Coupling Efficiency In Laser Surface Treatment *ISIJ International* **33** 925-933
[26] Kaplan A F H, Mizutani M, Katayama S and Matsunawa A 2002 Unbounded keyhole collapse and bubble formation during pulsed laser interaction with liquid zinc *J. Phys. D:Appl. Phys.* **35** 1218-1228
[27] Carslaw H S and Jaeger J C 1959 *Conduction of Heat in Solids 2nd ed.* (Oxford University Press, New York) pp.75
[28] Mundra K and Debroy T 1993 Calculation of Weld Metal Composition Change in High-Power Conduction Mode Carbon Dioxide Laser-Welded Stainless Steels. *Metall Trans* **24B** 145-155
[29] Aden M, Beyer E, Herziger G and Kunze H 1992 Laser-induced vaporization of a metal surface. *J. Phys. D: Appl. Phys.* **25** 57-65
[30] Aden M, Beyer E and Herziger G 1990 Laser-induced vaporization of metal as a Riemann problem. *J. Phys. D: Appl. Phys.* **23** 655-661
[31] Katayama S, Kobayashi Y, Mizutani M and Matsunawa A 2001 Effect of vacuum on penetration and defects in laser welding *J. Laser Appl.* **13** 187-192
[32] Mueller S and Bratt C 2010 Laser Beam Welding in Sub-Atmospheric Pressure *Proc. of the 29th ICALEO* (Anaheim CA) 1806
[33] Geiger M, Leitz K H, Koch H and Otto A. 2009 A 3D transient model of keyhole and melt pool dynamics in laser beam welding applied to the joining of zinc coated sheets. *Prod. Eng. Res. Devel.* **3** 127–136
[34] Petring D 1994 *Anwendungsorientierte Modellierung des Laserstrahl-schneidens zur rechnergestützten Prozeßoptimierung Ph. D. Thesis RWTH Aachen* (Aachen: Verlag Shaker)
[35] Mas C, Fabbro R and Gouedard Y 2003 Steady-state laser cutting modelling *J. Laser Applications* **15** 145-152
[36] Quintero F, Varas F, Pou J, Lusquinos F, Boutinguiza M, Soto R and Perez-Amor M 2005 Theoretical analysis of material removal mechanisms in pulsed laser fusion cutting of ceramics J. Phys. D: Appl. Phys. **38** 655-666
[37] Mas C 2003 *Modelisation physique du procede de decoupe de metaux par laser Ph. D. Thesis L'Universite Paris 6*
[38] Onuseit V, Ahmed M A, Weber R and Graf T 2011 Space-resolved Spectrometric Measurements of the Cutting Front *Physics Procedia* **12** 584-590
[39] Hirano K and Fabbro R 2011 Experimental investigation of hydrodynamics of melt layer during laser cutting of steel *J. Phys. D: Appl. Phys.* **44** 105502